3-15-2009

Inactivation of [Fe-Fe]-Hydrogenase by O2. Thermodynamics and Frontier Molecular Orbitals Analyses

Daniela Dogaru
Cleveland State University

Stefan Motiu
Cleveland State University

Valentin Gogonea
Cleveland State University, V.GOGONEA@csuohio.edu

Publisher's Statement

This is the accepted version of the following article: Dogaru, D.; Motiu, S.; Gogonea, V. Inactivation of [Fe-Fe]-hydrogenase by O2. Thermodynamics and frontier molecular orbitals analyses. International Journal of Quantum Chemistry 2009, 109, 876-889., which has been published in final form at: http://onlinelibrary.wiley.com/doi/10.1002/qua.21875/abstract

Inactivation of [Fe—Fe]-Hydrogenase by O_2. Thermodynamics and Frontier Molecular Orbitals Analyses

DANIELA DOGARU, STEFAN MOTIU, VALENTIN GOGONEA

Introduction

Both [Fe-Fe]-hydrogenases as well as [Ni-Fe]-hydrogenases are enzymes that are implicated in H_2 metabolism ($2H^+ + 2e^- \leftrightarrows H_2$), which occurs in anaerobic media. Of these two bi-metal enzymes, only [Fe-Fe]-hydrogenases are viable for H_2 production, with a reactivity of up to 2 orders of magnitude larger than [Ni-Fe]-hydrogenases [1, 2]. In hydrogenases, H_2 evolution, emerging from proton reduction ($2H^+ + 2e^- \rightarrow H_2$), is essential in pyruvate fermentation, and in the disposal of excess electrons. Low-molecular weight biomolecules such as ferredoxins, cytochrome C3, and cytochrome C6 can act as physiological electron acceptors or donors [3].

The hydrogenase H-cluster (Scheme 1) is the active site that is comprised of two subunits, the 2Fe subunit and the cubane $[Fe_4\text{-}S_4]^{2+}$ subunit. The 2Fe subunit is composed of two iron atoms (Fe_p-Fe_d, i.e., proximal and distal iron) that are bridged by di(thiomethyl)amine (DTMA) chain and are coordinated by endogenous ligands, i.e., two cyanides, two terminal carbonyls, and a bridging carbonyl (CO_b). Moreover, the S_γ (of Cys^{382}) is the connecting atom from an Fe atom of the (proximal) cubane subunit and the Fe_p of the 2Fe subunit.

The reason for studying biological H_2 production is because the eventual elucidation of the mechanism (for hydrogen synthesis) may benefit researchers produce clean fuel, using certain anaerobic prokaryotes [4–8].

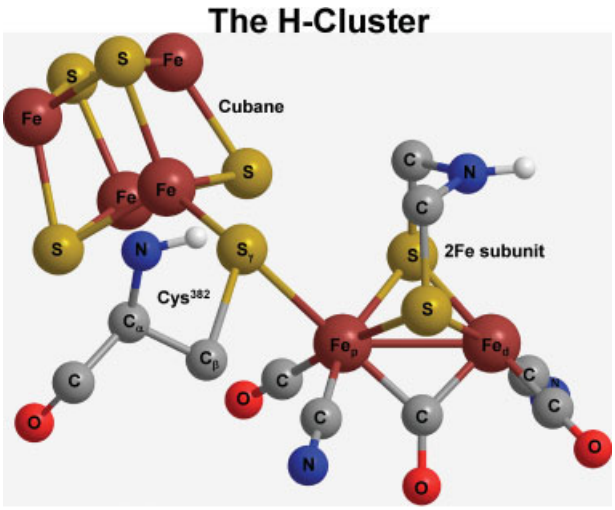

SCHEME 1. The H-cluster and its subunits, i.e., the cubane, and the 2Fe subunit. [Color figure can be viewed in the online issue, which is available at www.interscience.wiley.com.]

Previous density functional theory (DFT) as well as hybrid quantum mechanics/molecular mechanics (QM/MM) calculations [2, 9–16] have been successful in clarifying some aspects of the catalytic properties of the H-cluster.

As in similar computational studies [2, 9], cysteine is substituted with $CH_3\text{-}S^-$, whereas cubane is replaced[1] with a H^+.

Furthermore, computational and experimental [2, 9, 14, 16–41] [Fe-Fe]-hydrogenase H-cluster (and synthetic H-cluster-like compounds) research sheds light on the potential redox states of the 2Fe H-cluster subunit, Fe_p-Fe_d, where Fe_p^{I}-Fe_d^{I} is the reduced 2Fe H-cluster subunit, Fe_p^{II}-Fe_d^{I} is the partially oxidized enzyme subunit, and Fe_p^{II}-Fe_d^{II} is the fully oxidized, inactive enzyme H-cluster subunit.

The fully oxidized H-cluster, Fe_p^{II}-Fe_d^{II}, has a H_2O molecule or an OH^- bound to the Fe_d^{II}. In our previous investigation [21], we have inferred that a vacant (fully oxidized) Fe_p^{II}-Fe_d^{II} (1, Fig. 1) could also be a viable intermediate in H_2 synthesis. Regardless of the 2Fe H-cluster subunit redox states, the proximal cubane [more precisely, a cuboid (point group: D_2d)] always retains a 2+ oxidation state, $[Fe_4\text{-}S_4]^{2+}$.

The partially oxidized H-cluster (Fe_p^{II}-Fe_d^{I}, 5, Fig. 1), H_{ox}, is the active form of the hydrogenase enzyme.[2] The reduced H-cluster (Fe_p^{I}-Fe_d^{I}, 6, Fig. 1) has both iron atoms in oxidation states I (being an intermediate in H_2 metabolism). According to Liu and Hu [9], 6 is the cluster having great affinity for protonation ($6 \rightarrow 8$), in capturing a proton from the side chain of a near by amino-acid, such as Lys^{237}.

X-ray crystallography and spectroscopic studies of hydrogenases, with the latter having been obtained from *Clostridium pasteurianum* (CPI)[43] and *Desulfovibrio desulfuricans* (DdH) [31], led to a better understanding of the biochemical roles of these enzymes. The X-ray crystal structure of CPI hydrogenase shows an oxygen species that may be OH^-, or H_2O bound to the Fe_d of the H-cluster. On the basis of the computational results of Liu and Hu [2]

[1]The truncation of the cubane, $[Fe_4\text{-}S_4]^{2+}$, and its replacement by a H^+ (as well as the replacement of $CH_3\text{-}S^-$ for cysteine-S) had been done to obtain the best compromise with regard to the computational cost.

[2]Voltametric [42] studies show the transition of H_{ox}^{inact} to H_{ox}^{cat} occurring via a reversible e^- transfer process to the hydrogenase transient state followed by a putative two e^- transfer (with the latter not reaching the bimetals of the H-cluster).

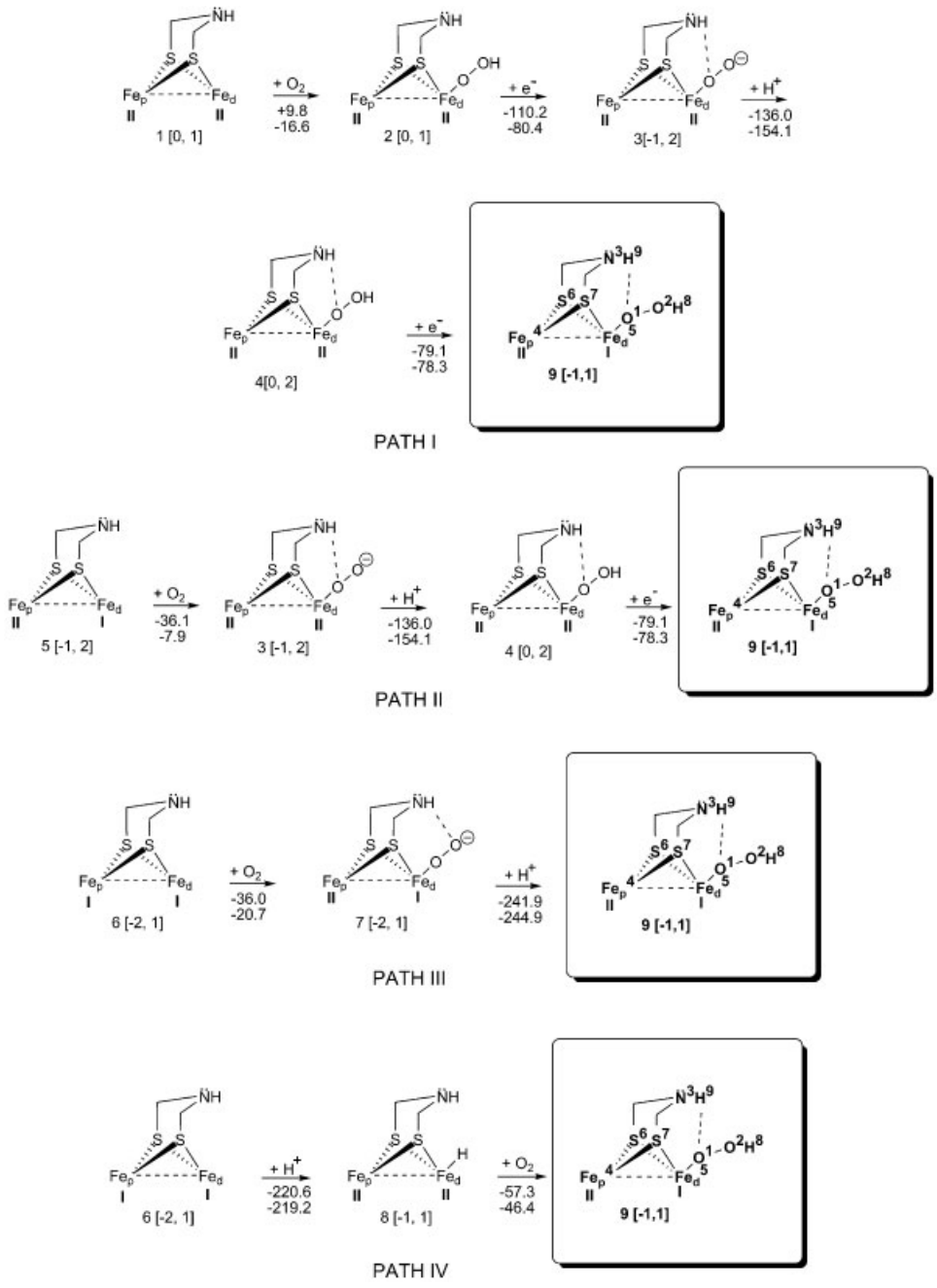

FIGURE 1. Reaction pathways I–IV: Oxidation mechanisms of H-clusters that are fully oxidized (1), partially oxidized (5), and reduced (6). The charges and multiplicities are given in square brackets. The first energy value is for gas phase, and the second is for ONIOM calculations. Fe_p is the proximal iron, and Fe_d is the distal iron.

(CPI has OH^- in its inactive form according to X-ray crystal structure), we endeavor to ascertain whether the air oxidized H-cluster (Fe_p-Fe_d-O_2) converts to Fe_p-Fe_d-OH species [21].

Our investigation is composed of three different subdivisions. (1) Thermodynamic analysis, for every reaction path mechanism (Figs. 1–3), implicated in the eventual H-cluster 14 inhibition by means of $O_2 \rightarrow OH^-$. (2) Electronic analysis, for the same paths, which deals with Natural Bond Orbitals (NBO), as well as Frontier Molecular Orbitals (FMO). (3) Geometrical analysis car-

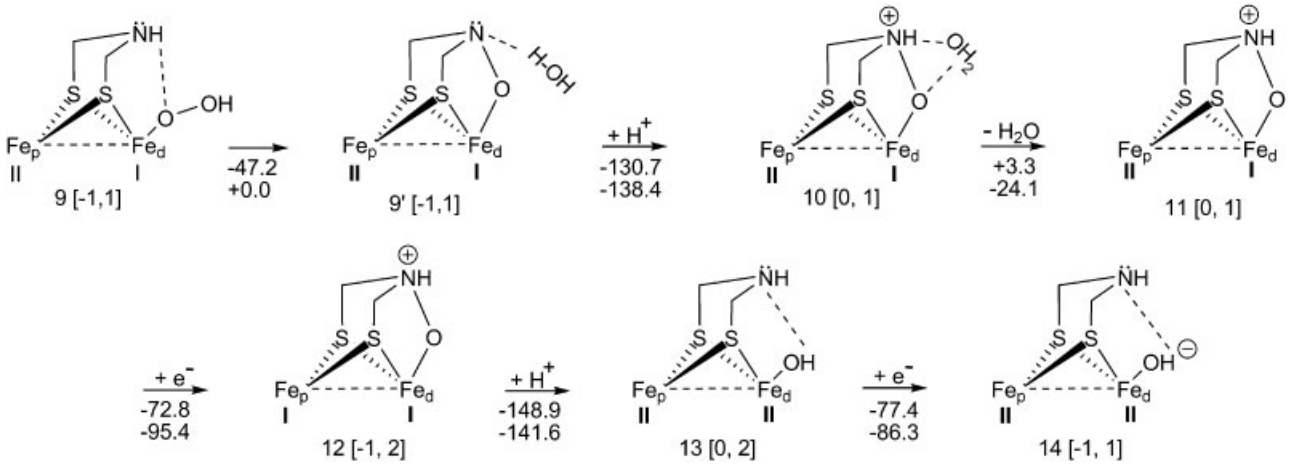

FIGURE 2. Reaction mechanism for isomerization, protonation, H_2O elimination, and reduction of the inhibited [Fe—Fe]-hydrogenase H-cluster. The H_2O is being removed from a closed-shell cluster. (The charges, multiplicities, and energy values are presented as in Fig. 1.)

ried out only for appropriate bond breaking and bond formation.

From the investigated subdivisions, thermodynamics analysis (Figs. 2 and 3) is of pivotal importance because it shows that there is just an exergonic path from H-cluster 9′ to the hydroxylated cluster 14 occurring in the aqueous enzyme phase. However, from the thermodynamic results (see Fig. 1), it is observed that most reaction steps proceed exergonically (except 1 → 2, gas phase), leading to the oxidized cluster 9. Moreover, at the end of each path, every vacant H-cluster 1, 5, and 6, in spite of its oxidation states, becomes aerobically inactivated, 9.

Thus, this article is organized as follows: in the Methods we describe the QM/MM partitioning, and the methods used for calculations (e.g., QM Hamiltonian, basis sets, and the force field param-

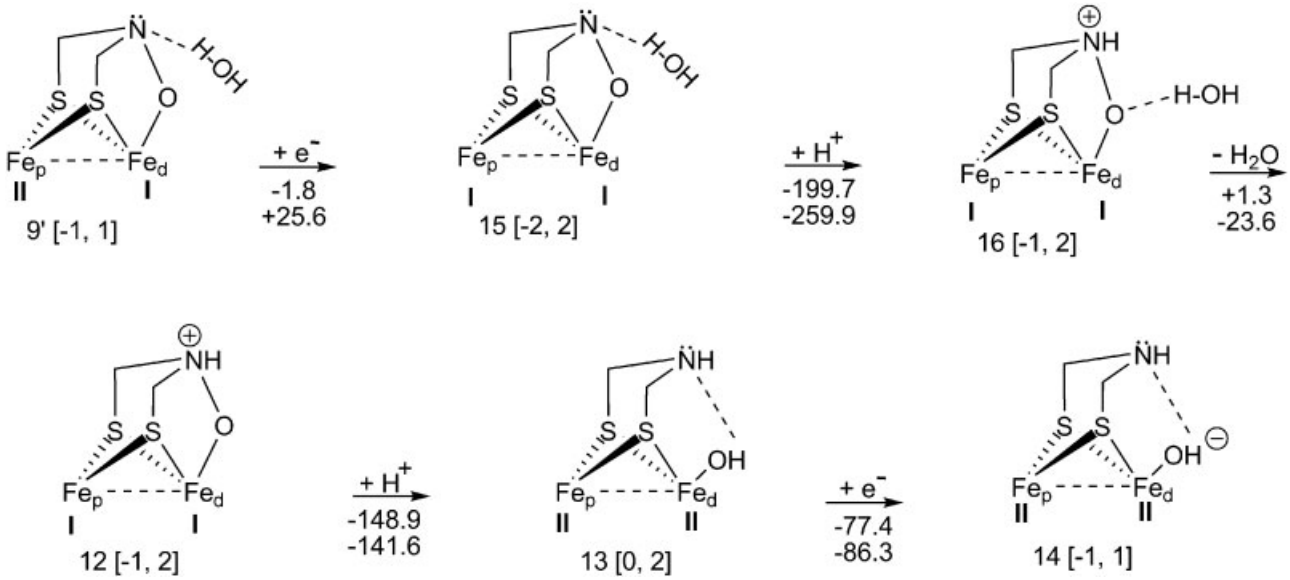

FIGURE 3. Reaction mechanism for reduction, protonation, and H_2O removal from the inhibited [Fe—Fe]-hydrogenase H-cluster. Here, the H_2O is being eliminated from an open-shell cluster. (The charges, multiplicities, and energy values are presented as in Fig. 1.)

eters). Then, in the Results and Discussion, we present the computational results organized into subsections that present and discuss thermodynamic results, geometrical, and electronic data for different steps of the reaction pathways, such as oxygen binding, reduction, oxidation, and water elimination. Finally, in the Conclusion we give a summary of our findings.

Methods

In this study, both QM [DFT (in gas phase)] and QM/MM [DFT/UFF [44] (in aqueous enzyme phase)] methodologies have been used. The ONIOM [45] method (DFT for the QM region and the universal force field (UFF) for the MM region, implemented in Gaussian 03 [46]) has been applied to determine the reaction thermodynamics, i.e., ΔG, for the inactivation pathways of the H-cluster, and the [Fe-Fe]-hydrogenase H-cluster (positioned within the enzyme matrix). Subsequently, the DFT results have been compared with the ONIOM calculations. The electronic structure of the hydrogenase active site (except the proximal cubane) is investigated by quantum mechanics (Gaussian 03) using DFT method (B3LYP functional [47, 48]), and QM/MM with 6-31+G(d,p) basis set. For Fe an effective-core potential with a double zeta polarization basis set (LANL2DZ [49, 50]) was used for DFT gas phase calculations, and a 6-31+G(d,p) basis set for the ONIOM calculations. In accordance with experimental and in-silico data low spin states (singlet and doublet) and low oxidation states (I and II) have been selected for the Fe atoms [2, 14, 35]. Gromacs program [51, 52] was employed to add hydrogen atoms, water, and counter ions to the X-ray crystal structure of DdH [Brookhaven Protein Data Bank id.1HFE]. Hydrogen atoms and a 1 nm layer of water (2043 molecules) have been added to the PDB DdH structure. Moreover, Na^+ ions have been randomly inserted into the solvent to neutralize the negative charges encountered therein, e.g., the -2 a.u. found on the cubane/cysteine moieties [53][3]. For both basic and acidic amino acids, charges were assigned by Gromacs algorithm to be at pH 7. ONIOM geometry optimizations have been performed on the DdH, with the low layer (MM region) being frozen,[4] with the exception of the proximal cubane, whereas the high layer (QM) had only the iron atoms, Fe_p-Fe_d, and the N3, (of the DTMA bridge) kept frozen; "freezing atoms" is practiced to reduce computational time. The low layer consists of all the hydrogenase amino acids as well as its constituent cubanes, i.e., proximal, medial, and distal. The high layer is comprised of 2Fe subunit (which is the moiety of the H-cluster) and C_β and S_γ (appertaining to the bridging Cys^{382}). Moreover, two linking hydrogen atoms were added between C_α and C_β of Cys^{382} and between S_γ and an Fe atom of the proximal cubane. The charge equilibration method of the UFF was used to describe the electrostatic interactions within the low layer of the system [54]. The DdH partial charges were obtained using the charge equilibration method, whereas the solvent charges were acquired from literature [54] ($q_O = -0.706$ a.u. and $q_H = 0.353$ a.u.).

Results and Discussion

H-CLUSTER THERMODYNAMICS FOR O_2 BINDING, REDUCTION, AND PROTONATION

Figure 1 illustrates different O_2 inhibition pathways of the hydrogenase H-cluster; the H-clusters, 1, 5, 6, and 8 [2, 9, 21], of the pathways are obtained in the reversible catalysis of H_2. Reaction $1 \rightarrow 2$ (path I) is endergonic for the gas phase ($\Delta G_{gas} = +9.8$ kcal/mol; gas = gas phase) when O_2 binds to the fully oxidized H-cluster (1). ONIOM calculations, on the other hand, show that O_2 binding occurs exergonically ($\Delta G_{QM/MM} = -16.6$ kcal/mol), shedding light on the sensitivity of hydrogenases to O_2 [55].

Reduction $2 \rightarrow 3$ ($\Delta G_{gas} = -110.2$ kcal/mol) as well as protonation $3 \rightarrow 4$ ($\Delta G_{gas} = -136.0$ kcal/mol) proceed exergonically; ONIOM calculations, for the hydrogenase matrix, show that e^- transfer is considerably less exergonic ($\Delta G_{QM/MM} = -80.4$ kcal/mol) relative to protonation which is more exergonic ($\Delta G_{QM/MM} = -154.1$ kcal/mol). The free energy differences, in gas versus aqueous enzyme phases for reactions $2 \rightarrow 3$ and $3 \rightarrow 4$, ensue from the effect of the electric field of the protein on the H-clusters 2, 3, and 4, and from the different phase geometries.

Cluster 4 undergoes reduction and it ($4 \rightarrow 9$) proceeds exergonically in both gas and aqueous

hydrogenase phase (ΔG_{gas} = −79.1 kcal/mol; $\Delta G_{QM/MM}$ = −78.3 kcal/mol).

Path II starts with the partially oxidized H-cluster 5, (Fe_p^{II}-Fe_d^{I}). The binding of O_2 to Fe^{I} (Fe_d^{I}-O_2), 5 → 3, is firmer (ΔG_{gas} = −36.1 kcal/mol) than for Fe^{II} in 1 → 2 (Fe_d^{II}-O_2, path I). In contrast, ONIOM results show that O_2 binds to the partially oxidized H-cluster (Fe_p^{II}-Fe_d^{I}, $\Delta G_{QM/MM}$ = −7.9 kcal/mol) as well as to the fully oxidized cluster (Fe_p^{II}-Fe_d^{II}, $\Delta G_{QM/MM}$ = −16.6 kcal/mol, 1 → 2, path I). The remaining two reactions 3 → 4, and 4 → 9 (path II) are the same as the last two steps of path I.

In path III, 6 → 7, which starts with the fully reduced H-cluster 6, (Fe_p^{I}-Fe_d^{I}), the reaction spontaneity (ΔG_{gas} = −36.0 kcal/mol) is almost identical to the free energies of reaction 5 → 3. The gas phase free energy similarity may ensue because both loci of oxygen binding (Fe_d^{I}-O_2) are on similar oxidized species, Fe_d^{I}. However, ONIOM calculations show smaller reaction spontaneity difference between aqueous enzyme ($\Delta G_{QM/MM}$ = −20.7 kcal/mol) and gas phase results (ΔG_{gas} = −36.0 kcal/mol, 6 → 7), than for O_2 binding in path I and II. In path III, protonation (7 → 9) is, once again, largely exergonic for both phases (ΔG_{gas} = −241.9 kcal/mol; $\Delta G_{QM/MM}$ = −244.9 kcal/mol). Moreover, from all of Figure 1, the above ONIOM calculations show the highest H^+ affinity because H-cluster 7 has a charge of −2 a.u., and also the H^+ binds to a rather electronegative atom, viz., oxygen.

In the final path (IV), protonation 6 → 8 is the second most exergonic reaction in gas phase (ΔG_{gas} = −220.6 kcal/mol) mostly because of the over-all charge of −2 on the H-cluster 6. ONIOM data (as in 7 → 9) show very high H^+ affinity ($\Delta G_{QM/MM}$ = −219.2 kcal/mol) for the hydrogenase H-cluster (in spite of the fact that the H^+ is seized by the Fe_d as opposed to the more electronegative Fe_d-O_2, 7 → 9), which is comparatively similar to the gas phase result (ΔG_{gas} = −220.6 kcal/mol).

In the last step (8 → 9; path IV), O_2 is interposed between Fe_d and the hydride (Fe_d^{I}-O_2-H, 9). For this insertion reaction, the O_2 binding occurs exergonically in both ONIOM ($\Delta G_{QM/MM}$ = −46.4 kcal/mol) and the gas phase (ΔG_{gas} = −57.3 kcal/mol) results.

NB: Path IV shows that oxidation of Fe_p-Fe_d H-cluster is similar[5] to the Ni_p-Fe_d hydrogenase H-cluster obtained from experimental data [56].

From the earlier thermodynamic results, most reaction steps proceed exergonically (except 1 → 2, gas phase), leading to oxidized cluster 9. At the end of every path, each vacant H-cluster 1, 5, or 6, in spite of its oxidation states, becomes aerobically inactivated.

NBO CHARGES AND GEOMETRY ADJUSTMENT OF INTERMEDIATES IN THE OXIDATION OF H-CLUSTER

The atoms of the vacant H-clusters 1, 5, and 6 have slightly different natural bond orbital (NBO) charge distributions. For instance, for cluster 1 the NBO charges of Fe_p-Fe_d are q^g_{Fep}[6] = 0.137 a.u. (q^e_{Fep} = −0.230 a.u.) and q^g_{Fed} = −0.096 a.u. (q^e_{Fed} = 0.187 a.u.), whereas in 5, the sign of the partial charges are reversed only in gas phase, i.e. q^g_{Fep} = −0.024 a.u. (q^e_{Fep} = −0.227 a.u.) and q^g_{Fed} = 0.078 a.u. (q^e_{Fed} = 0.061 a.u.). Then, the NBO charges for the Fe_p-Fe_d in cluster 6 (in both phases) are more negative, q^g_{Fep} = −0.104 a.u. (q^e_{Fep} = −0.297 a.u.) and q^g_{Fed} = −0.117 a.u. (q^e_{Fed} = −0.160 a.u.) because both metals are in a reduced state (see Fig. 1), unlike clusters 1 and 5. Regarding charges on the nitrogen, N3, (of the DTMA bridge), similarities are seen among clusters 1, 5, and 6; the NBO charges for N3 are approximately −0.700 a.u., making this amine (within the above H-clusters) a relatively important H^+ acceptor/donor (vs. amino acids with similar function in the juxtaposed enzyme matrix, e.g., Lys^{237}) as suggested by Liu and Hu [9]. The nonbridging S_γ (of Cys^{382}) has the following charges: for 1 $q^g_{S\gamma}$ = 0.204 a.u. ($q^e_{S\gamma}$ = 0.474 a.u.), for 5 $q^g_{S\gamma}$ = 0.142 a.u. ($q^e_{S\gamma}$ = 0.425 a.u.), and for 6 $q^g_{S\gamma}$ = 0.079 a.u. ($q^e_{S\gamma}$ = 0.285 a.u.). Comparing clusters 1, 5, and 6, a sequential drop in NBO charges for Fe_p and S_γ is observed.

When H-cluster 1 is in an oxidized state (in gas phase), Fe_p^{II}- Fe_d^{II}, the CO_b shifts [9] towards the Fe_d^{II} and becomes bonded to Fe_d^{II}. The shifted CO_b bond distance (measured from its bridging carbon, C_b, to the iron atoms) between C_b-Fe_p^{II} is 3.067 Å, whereas C_b-Fe_d^{II} is 1.819 Å. When the carbonyl is close to Fe_d^{II}, CO_b-Fe_d^{II}, the fully oxidized H-cluster 1 becomes relatively stable versus the quasi-symmetric cluster [21] (ΔH = 14 kcal/mol), which is also shown by the NBO charge on C_b in CO_b, (0.664 a.u.). This may be due to repulsion of charges be-

tween q^g_{Cb} (0.664 a.u.) and q^g_{Fep} (0.137 a.u.), whereas for the clusters 5 and 6, the partial charges (q^g_{Cb} = 0.462 a.u. and q^g_{Cb} = 0.466 a.u., respectively) are less then in 1 because CO_b is bonded to both iron atoms. However, in the enzyme phase less shifting of the bridging carbonyl occurs, with the charges on C_b being similar (q^e_{Cb} = 0.536 a.u. for 1, q^e_{Cb} = 0.497 a.u. for 5, and q^e_{Cb} = 0.493 a.u. for 6). Comparing the reaction spontaneity for O_2 binding (in gas phase), which renders clusters 2, 3, and 7, one may observe that 3 and 7 are more stable than 2. The reason for this stability is essentially due to the formation of a hydrogen bond between the exogenous O_2 and the hydrogen H9 (bonded to N3 of the DTMA bridge) in both 3 and 7. The O1—H9 bond distance is 2.016 Å in 3, and O2—H9 bond distance is 1.765 Å in 7, which correlates with the NBO charges on the mentioned oxygens and hydrogens; the partial charges on oxygens are q^g_{O1} = −0.235 a.u. in 3 and q^g_{O2} = −0.493 a.u. in 7, whereas the charge on H9 is 0.439 a.u. in 3, and 0.454 a.u. in 7. Note that CO_b is located almost symmetrically in clusters 2, 3, and 7. Structurally, clusters 4 and 9 are similar in view of the fact that both possess a hydrogen bond (H9. . . O1), whereas CO_b is found to reside quasi-symmetrically in 9, but asymmetrically in 4 bonded only to Fe_p^{II}. In the enzyme phase both hydrogen bonds (in clusters 3 and 7) are formed between H9 and O2 of the exogenous oxygen (q^e_{O2} = −0.210 a.u. in 3, q^e_{O2} = −0.452 a.u. in 7, q^e_{H9} = 0.443 a.u. in 3, and q^e_{H9} = 0.445 a.u. in 7; O2—H9 bond distance is 1.890 Å in 3, and O2—H9 bond distance is 1.760 Å in 7).

THERMODYNAMICS AND NBO CHARGES RELATIONSHIP FOR H_2O REMOVAL FROM THE OXIDIZED H-CLUSTER

Figure 2 depicts a series of reactions (9 → 9′, 9′ → 10, 10 → 11, 11 → 12, 12 → 13, and 13 → 14), which present the net conversion of 9 to 14. The compounds 9 and 9′ are isomers; 9′ is more stable by 47.2 kcal/mol, [which may be, to a certain extent, attributed to the hydrogen bond formation between H_2O and the N3 of DTMA bridge (N3. . . H—OH; i.e., two bonds being broken vs. three being formed for 9 → 9′, respectively)]. The hydrogen bond length, N3. . . H, is 1.939 Å (and the angle formed by N3. . . H—O is 168.7°). The distance between the iron atoms is larger in 9′ (2.796 Å) than in 9 (2.605 Å). During reaction 9 → 9′, CO_b moves away from Fe_p^{II} [i.e., for C_b-Fe_p^{II} 2.225 Å (9) → 2.771 Å (9′)]. Also, in Figure 2 (hydrogenase H-cluster 9, and 9′), ONIOM geometry optimizations for 9, and 9′ resulted in the same structure for the hydrogenase H-clusters ($\Delta G_{QM/MM}$ corresponding to 9 → 9′ is 0 kcal/mol). The protonation of 9′ (9′ → 10) produces a quaternary ammonium ion (NR_4^+) within the DTMA bridge, which is exergonic for both phases, viz., ΔG_{gas} = −130.7 kcal/mol and $\Delta G_{QM/MM}$ = −138.4 kcal/mol. To wit, the observed high reaction spontaneity for both phases is attributed to the negatively charged H-cluster 9′. In 10 → 11, H_2O is removed from N3 by means of hydrogen bond breaking; this reaction (vs. 9′ → 10) occurs slightly endergonically in gas phase (ΔG_{gas} = +3.3 kcal/mol), whereas for QM/MM results, the H_2O removal step, 10 → 11, is exergonic ($\Delta G_{QM/MM}$ = −24.1 kcal/mol).

Reduction 11 → 12 (see Fig. 2) is subjected to an increase in the partial charge of the exogenous oxygen (q^g_{O1} = −0.568 a.u. (11) → −0.594 a.u. (12); ΔG_{gas} = −72.8 kcal/mol). Regarding geometrical changes in 11 → 12, the bond distance between Fe_p^{II}-Fe_d^{I} is increasing from 2.792 Å to 3.261 Å, whereas the CO_b departs from Fe_p^{II} [for C_b-Fe_p^{II} 2.766 Å (11) → 3.188 Å (12)]. For the aqueous enzyme phase result, 11 → 12 occurs with a relatively large free energy ($\Delta G_{QM/MM}$ = −95.4 kcal/mol; compared with other neutral H-cluster reductions), versus the gas phase outcome (ΔG_{gas} = −72.8 kcal/mol); the charge remains constant on the exogenous oxygen [q^e_{O1} = −0.530 a.u. (11) → −0.527 a.u. (12)]. Because of excess electron density accumulation on O1 (12), the latter readily captures a proton (12 → 13; ΔG_{gas} = −148.9 kcal/mol). ONIOM calculations, 12 → 13, confirm the high H^+ affinity (in Fig. 2, $\Delta G_{QM/MM}$ = −141.6 kcal/mol) for the hydrogenase H-cluster, which is close to the gas phase result (ΔG_{gas} = −148.9 kcal/mol). The free energy differences between the given protonations, 12 → 13 versus 9′ → 10, may arise because of the greater stability of cluster 13 versus 10.

Finally, in Figure 2, an e^- is acquired by the hydroxyl group (13 → 14; ΔG_{gas} = −77.4 kcal/mol; $\Delta G_{QM/MM}$ = −86.3 kcal/mol). Note that the H-cluster 14 [2, 21] is the starting compound in the reactivation pathway that ends in the reduced H-cluster 6 (Fe_p^{I}-Fe_d^{I}).

In Figure 3, an alternative pathway (9′ → 15, 15 → 16, 16 → 12, 12 → 13, and 13 → 14) has been investigated. The pathway starts with a reductive step, rather than with a protonation. Reaction 9′ → 15 is slightly exergonic for the gas phase (ΔG_{gas} = −1.8 kcal/mol), whereas ONIOM calculations indi-

cate an endergonic process ($\Delta G_{QM/MM}$ = +25.6 kcal/mol). 9′ → 15 is another O_2 inhibitory step (in addition to 10 → 11 for the gas phase, Fig. 2) which seems to explain the O_2 sensitivity of wild type DdH. Therefore, mutagenic studies ought to be performed on [Fe-Fe]-hydrogenase H-cluster 9′ to eliminate its inhibitory path (viz., 9′ → 15). When a H^+ is in the vicinity of H-cluster 15, 15 → 16 proceeds with the greatest spontaneity (of Figs. 2 and 3) in gas phase (ΔG_{gas} = −199.7 kcal/mol) because 15 has a net charge of −2 a.u. Note that the ONIOM findings, for step 15 → 16, confirm the highest free energy ($\Delta G_{QM/MM}$ = −259.9 kcal/mol) of all the potential reaction mechanisms analyzed for the [Fe—Fe]-hydrogenase H-cluster, whereas the gas phase result is about 60 kcal/mol less exergonic. Water elimination in gas phase, (16 → 12) is slightly endergonic (ΔG_{gas} = +1.3 kcal/mol), whereas for the aqueous enzyme phase it is significantly exergonic ($\Delta G_{QM/MM}$ = −23.6 kcal/mol). Note that both 10 (see Fig. 2) and 16 (see Fig. 3) lead to the same compound (12) by H_2O elimination. The thermodynamic data are similar for both reactions, 10 → 11 and 16 → 12, because Fe_d is found in the same oxidation state (Fe_d^I) in both 10 and 16, but Fe_P (being further away from the focal catalytic locus, Fe_d) has different oxidation states [Fe_P^{II} (10); Fe_P^I (16)]. The in silico ONIOM result of the H_2O removal step (Fig. 3, 16 → 12), is exergonic ($\Delta G_{QM/MM}$ = −23.6 kcal/mol), just like in step 10 → 11, (Fig. 2, $\Delta G_{QM/MM}$ = −24.1 kcal/mol). Also, close free energies are observed for the gas phases of 16 → 12 (ΔG_{gas} = +1.3 kcal/mol) and 10 → 11 (ΔG_{gas} = +3.3 kcal/mol). Next, reactions 12 → 13 and 13 → 14 proceed exergonically [(ΔG_{gas} = −148.9 kcal/mol; $\Delta G_{QM/MM}$ = −141.6 kcal/mol) and (ΔG_{gas} = −77.4 kcal/mol; $\Delta G_{QM/MM}$ = −86.3 kcal/mol), respectively], just as (previously discussed) in Figure 2. The following reactions, 10 → 11 (see Fig. 2) and 16 → 12 (see Fig. 3), show that the entire (oxidative inhibitory H-cluster) path has difficulties proceeding to 14 in gas phase.

From the earlier discussion, it can be seen that there is only one exergonic path (see Fig. 2) from the oxidized H-cluster 9′ to the hydroxylated cluster 14 in aqueous enzyme phase. A path starts with H^+ transfer (see Fig. 2), whereas the other begins by e^- transfer (see Fig. 3). The gas phase H_2O elimination, from the oxidized H-cluster, proceeds endergonically in both pathways (Figs. 2 and 3).

FRONTIER MOLECULAR ORBITAL ANALYSIS

Electronic contributions are now presented for both phases, which are adduced by the frontier molecular orbitals in conjunction with the previously presented free energies.

Upon reduction of open-shell H-clusters, it is observed that an e^- is obtained by a semi-occupied molecular orbital (SOMO), whereas the closed-shell clusters receive an e^- into the lowest virtual molecular orbital (LUMO). However, when a H^+ is in the proximity of an open-shell H-cluster, it can form a σ-bond probably through the interaction of the e^- in the highest occupied molecular orbital (HOMO), or through the contributions of both HOMO and SOMO, with the proviso that the SOMO is sufficiently low in energy relative to HOMO. Alternatively, when a H^+ is near a closed-shell cluster, the σ-bond probably ensues mainly due to the contribution of e^-s from HOMO with the H^+.

Gas phase thermodynamic properties, of the reactions in Figures 1–3, are being examined with regard to frontier molecular orbitals (FMO) shown in Figs. 4 and 5. Thus, in 2 the LUMO (see Fig. 4) is mostly localized on the exogenous O_2 and N3, which is also corroborated by an increase of NBO charges on O_2 and N3 in 3 upon reduction of H-cluster 2 [q^g_{O1} = −0.046 a.u. (2) → −0.235 a.u. (3); q^g_{N3} = −0.568 a.u. (2) → −0.717 a.u. (3)].

Aqueous enzyme phase thermodynamic properties are next being examined for the reactions of Figures 1–3 relative to the frontier molecular orbitals (FMO).

For 2, LUMO [Fig. 6 (compare to Fig. 4 in gas phase)] is mostly localized on Sγ of Cys^{382} (as opposed to cluster 2 in gas phase) owing to the electronic contribution of the proximal cubane. Additionally, the localization of LUMO is supported by a decrease of NBO charge on Sγ in 3 upon reduction of H-cluster 2 [$q^e_{S\gamma}$ = 0.471 a.u. (2) → 0.388 a.u. (3)].

For open-shell clusters, unrestricted B3LYP calculations have been performed which resulted in different quantum mechanical (QM) energies and molecular orbital (MO) coefficients for α and β electrons.

In gas phase, the $HOMO_\alpha$ (the lower energy HOMO containing a spin up e^-) of 3 is predominantly localized on the exogenous O_2, where the protonation also occurs. However, the $HOMO_\beta$ (the higher energy HOMO with its spin down e^-) is localized on the DTMA bridge (see Fig. 4).

For the aqueous enzyme phase, the $HOMO_\alpha$ of 3 is less localized on the exogenous O_2 (relative to the

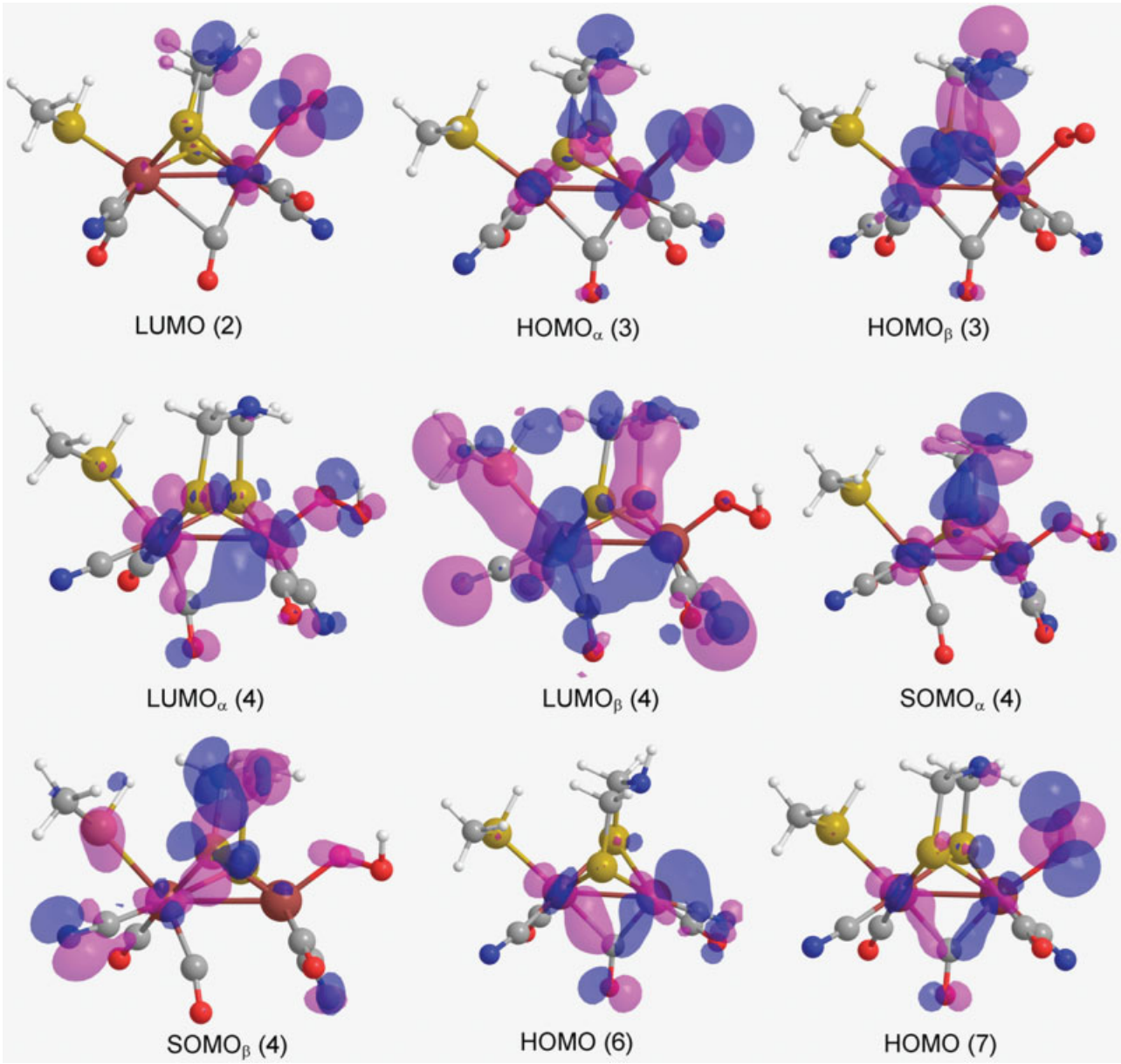

FIGURE 4. Frontier molecular orbitals (gas phase) for H-clusters LUMO (2), $HOMO_{\alpha}$ (3), $HOMO_{\beta}$ (3), $LUMO_{\alpha}$ (4), $LUMO_{\beta}$ (4), $SOMO_{\alpha}$ (4), $SOMO_{\beta}$ (4), HOMO (6), and HOMO (7) (where the atom colors, of the H-clusters, are O, red; C, gray; N, blue; S, yellow; Fe, burgundy; and H, white). [Color figure can be viewed in the online issue, which is available at www.interscience.wiley.com.]

gas phase situation), but this orbital is essentially localized on the DTMA bridge.

The $HOMO_{\beta}$, relative to the gas phase electronic distribution, is more localized on the exogenous O_2 (see Fig. 6), supporting the greater spontaneity of H^+ transfer ($3 \rightarrow 4$).

The $SOMO_{\alpha}$ of compound 4, in gas phase, is mostly localized on the DTMA bridge, and, to some extent, on the exogenous O_2 and the Fe atoms (see Fig. 4). $SOMO_{\beta}$ is more delocalized than $SOMO_{\alpha}$. Following the e^- transfer $4 \rightarrow 9$, the main change in partial charges occurs on the iron atoms $\{q^g_{Fep} = -0.141$ a.u. (4) $\rightarrow -[0.003$ a.u. (9); $q^g_{Fed} = 0.464$ a.u. (4) $\rightarrow 0.025$ a.u. (9)]$\}$ The change in NBO charges in $4 \rightarrow 9$ can be corroborated by $LUMO_{\alpha}$ (4; Fig. 4). It is noteworthy that the e^- is transferred into the

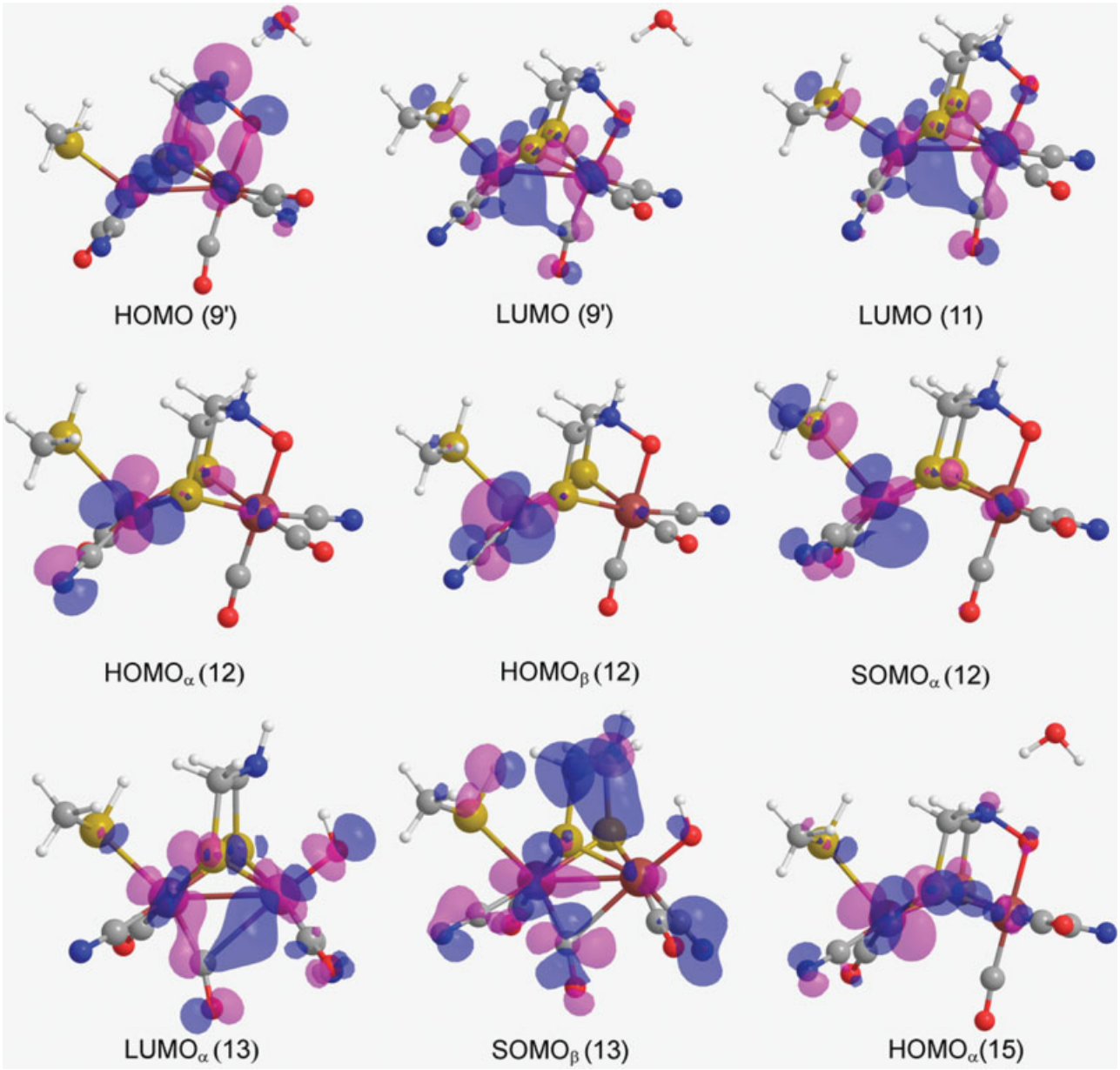

FIGURE 5. Frontier molecular orbitals (gas phase) for H-clusters HOMO (9′), LUMO (9′), LUMO (11), HOMO$_\alpha$ (12), HOMO$_\beta$ (12), SOMO$_\alpha$ (12), LUMO$_\alpha$ (13), SOMO$_\beta$ (13), and HOMO$_\alpha$ (15). [Color figure can be viewed in the online issue, which is available at www.interscience.wiley.com.]

LUMO$_\alpha$ (−0.15381 Hartrees), for its energy is lower than that of SOMO$_\beta$ (−0.14425 Hartrees). For the hydrogenase, LUMO$_\alpha$ (4, Fig. 6) is also lower in energy than SOMO$_\beta$ (4, Fig. 6) ($E_{\mathrm{LUMO}\alpha}^{\mathrm{Enzyme}} = -0.35944$ Hartrees, $E_{\mathrm{SOMO}\beta}^{\mathrm{Enzyme}} = -0.35907$ Hartrees), implying that the e^- is transferred to and localized on S_γ of Cys^{382}. However, this difference in electron localization is not reflected in the reaction thermodynamics, because 4 → 9 is similarly exergonic in both phases.

The HOMO of 6, in gas phase, is localized on the Fe_d and the CO_b, whereas the HOMO of 7 is primarily localized on the exogenous O_2 but is less diffused over CO_b (see Fig. 4). The proton binds with high affinity to Fe_d of H-clusters 6 (Path IV) and 7 (Path III) because the HOMO orbitals of these

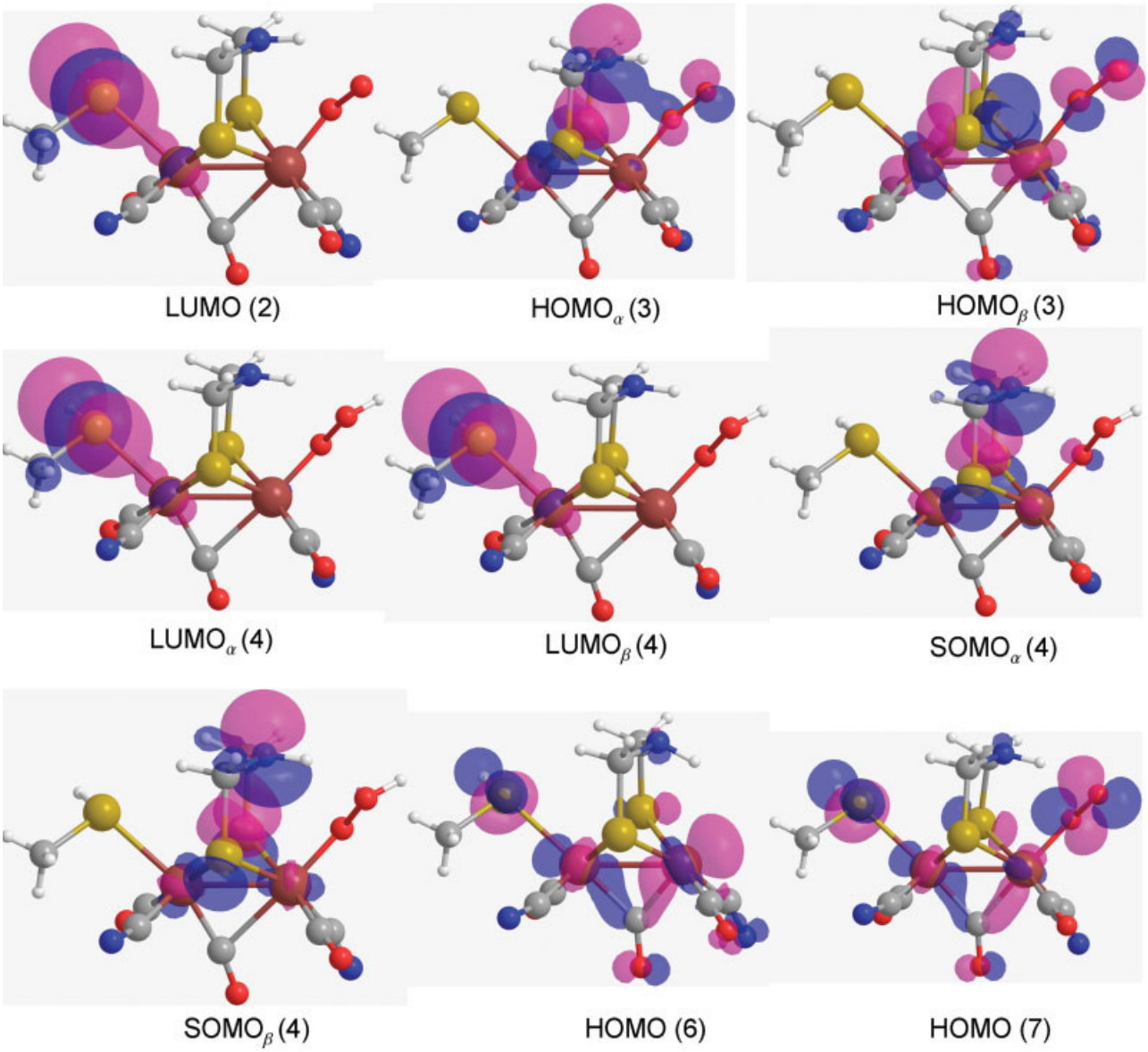

FIGURE 6. Frontier molecular orbitals (aqueous enzyme phase) for H-clusters LUMO (2), HOMO$_\alpha$ (3), HOMO$_\beta$ (3), LUMO$_\alpha$ (4), LUMO$_\beta$ (4), SOMO$_\alpha$ (4), SOMO$_\beta$ (4), HOMO (6), and HOMO (7). [Color figure can be viewed in the online issue, which is available at www.interscience.wiley.com.]

clusters are localized on Fe_d and exogenous O_2, respectively. In particular, 7 manifestly displays where protonation occurs, viz., on the exogenous O_2 (see Fig. 1).

In aqueous enzyme phase, similar electron orbital distributions are encountered for clusters 6 (Path IV) and 7 (Path III), except that S_γ (of Cys^{382}) incurs MO distributions, which may be sustained by the proximal cubane (that facilitates the e^- transfer).

The HOMO of 9′, is delocalized throughout the cluster and, has smaller proton affinity in comparison to 6 and 7. However, higher HOMO 9′ amplitude is found on the exogenous O1, DTMA bridge, and the two irons which may explain why the N3 is being protonated in this case.

For cluster 11, the LUMO is more localized over the Fe_p than on Fe_d, extending from the irons towards the CO_b via a linear combination between the e_g orbitals of the iron atoms with the CO_b π

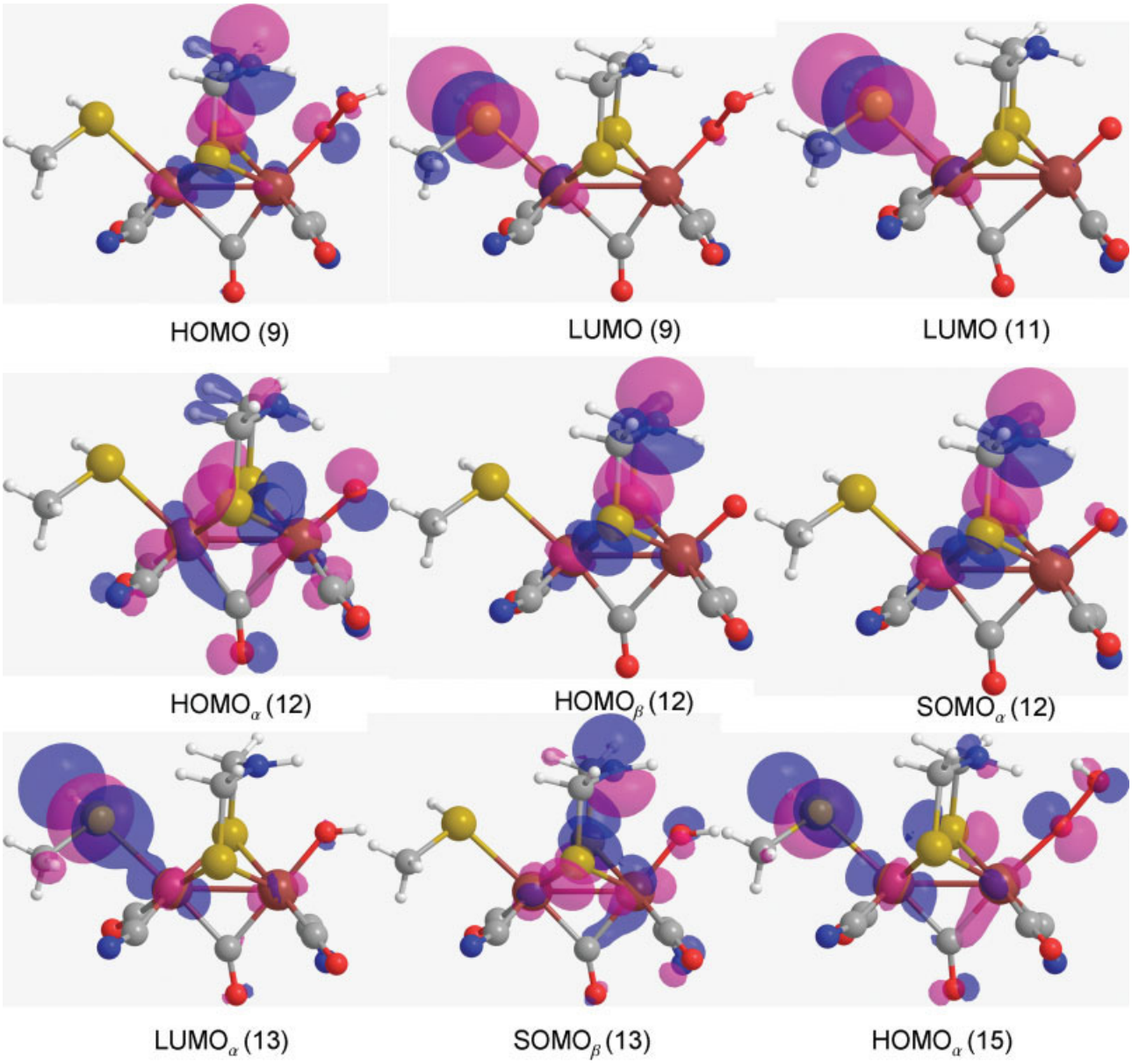

FIGURE 7. Frontier molecular orbitals (aqueous enzyme phase) for H-clusters HOMO (9), LUMO (9), LUMO (11), HOMO$_\alpha$ (12), HOMO$_\beta$ (12), SOMO$_\alpha$ (12), LUMO$_\alpha$ (13), SOMO$_\beta$ (13), and HOMO$_\alpha$ (15). [Color figure can be viewed in the online issue, which is available at www.interscience.wiley.com.]

orbitals [9], thus the e^- transfer, 11 → 12, changes the oxidation state of Fe_p. However, for ONIOM, the LUMO is localized on S_γ which is being bereft of e^-s via an inductive effect of the vicinal cubanes [$q^e_{S\gamma}$ = 0.464 a.u. (11) vs. 0.333 a.u. (12)].

Both HOMO$_\alpha$ and HOMO$_\beta$, of 12, are generally localized on the Fe_p (see Fig. 5). However, in this case, the protonation does not occur at the Fe_d, instead it occurs at the exogenous O1 because its NBO charge is very negative, i.e., $q^g_{O1} = -0.594$ a.u. as opposed to $q^g_{Fed} = 0.126$ a.u. On the other hand, for the aqueous enzyme phase, both HOMO$_\alpha$ and HOMO$_\beta$, of 12, differ in their distribution, especially HOMO$_\alpha$ having orbital amplitude on the exogenous oxygen, making it a good H^+ acceptor.

Cluster 13 is an open-shell cluster, so upon its reduction an e^- may either enter a LUMO$_\alpha$, or a SOMO$_\beta$ depending on their relative orbital ener-

gies. In the reductive process of H-cluster 13 (for gas phase), the in silico data explicitly shows that the orbital energy of $LUMO_\alpha$ ($E_{LUMO\alpha}^{gas}$ = −0.14850 Hartrees) is lower than the energy of $SOMO_\beta$ ($E_{SOMO\beta}^{gas}$ = −0.13886 Hartrees). Nevertheless, these energies are almost identical in the aqueous enzyme phase ($E_{LUMO\alpha}^{enzyme}$ = −0.35177 Hartrees, $E_{SOMO\beta}^{enzyme}$ = −0.35185 Hartrees). Thus, upon reduction of cluster 13, the e^- could enter into $LUMO_\alpha$ (Figs. 5 and 7 of both phases). Upon analysis of the NBO charges of clusters 13 and 14, the OH^- and Fe_d of 14 acquire most of the partial charge ceded by Fe_p during the reductive process 13 → 14.

Finally, in gas phase H-cluster 15 undergoes a protonation reaction on N3, which is substantiated by the NBO negative charge decrease, for both phases, on N3 [q^g_{N3} = −0.267 a.u. (15) → −0.187 a.u. (16)], while in protein environment the exogenous O_2 is protonated [q^e_{O2} = −0.510 a.u. (15) → −1.024 a.u. (16)].

Conclusion

Several possible pathways have been investigated for the oxidation of [Fe—Fe]-hydrogenase H-cluster, and they all proceed spontaneously to cluster, 9. Each pathway is initiated by an intermediate (1, 5, 6, and 8) of the catalytic cycles in H_2 metabolism.

In gas phase, O_2 binding is endergonic for the fully oxidized H-cluster 1 and exergonic for 8; however, it is exergonic for the partially oxidized 5 and reduced 6 clusters. But for aqueous enzyme phase, the O_2 binding is exergonic for all oxidation states. This suggests that the fully oxidized state of the H-cluster 1 in enzyme environment is more sensitive to O_2 inhibition.

Our calculations show that in the protein environment (Figs. 2 and 3) the hydroxylated H-cluster 14, which is the end product of hydrogenase inhibition,[7] is obtained from 9 via the fully exergonic reaction pathway that starts by means of protonation (see Fig. 2). Antithetically, the reaction pathway that is initiated by means of reduction (Fig. 3, aqueous enzyme phase) does not proceed to the hydroxylated H-cluster 14 due to this very endergonic step ($\Delta G_{QM/MM}$ = +25.6 kcal/mol).

The inhibitory steps in gas phase (Figs. 2 and 3) consist of water removal from a closed shell, 10, and an open shell, 16, H-cluster (ΔG_{gas} = +3.3 and +1.3 kcal/mol, respectively), whereas in the aqueous enzyme phase there is one inhibitory step, i.e., an e^- transfer from an open shell H-cluster (9′, $\Delta G_{QM/MM}$ = +25.6 kcal/mol).

From gas phase geometrical analysis CO_b shows a displacement away from Fe_p^{II} (9 → 9′), but in the aqueous enzyme phase this CO_b translocation is not observed; the observed different phase behavior in the protein environment may be due to the imposed immobility on the iron atoms (by means of "freezing" them).

For the gas phase, cluster 11, LUMO is more localized over the Fe_p than on Fe_d, extending from the iron atoms towards the CO_b via a linear combination between the e_g orbitals of the iron atoms with the CO_b π orbitals [9], thus the e^- transfer, 11 → 12, changes the oxidation state of Fe_p. However, for the protein environment, the LUMO is localized on S_γ which is being bereft of e^-s via an inductive effect of the vicinal cubanes [$q^e_{S\gamma}$ = 0.464 a.u. (11) vs. 0.333 a.u. (12)].

Lastly, an interesting result from the FMO gas phase analysis is that an e^- is transferred to the $LUMO_\alpha$ rather than to the virtual $SOMO_\beta$, which is rather unexpected because the virtual $SOMO_\beta$ usually resides in a lower energy state than $LUMO_\alpha$ for open-shell compounds. We also found that O_2 inhibited [Fe—Fe]-hydrogenase H-cluster has OH^- bonded to the Fe_d, and that OH^- is the end product of O_2 metabolism, with all aqueous enzyme phase reaction pathways proceeding exergonically.

ACKNOWLEDGMENT

The authors acknowledge for the computational resources provided by the National Center for Supercomputer Applications (University of Illinois) and the Ohio Supercomputer Center.

References

1. Das, D.; Dutta, T.; Nath, K.; Kotay, S. M.; Das, A. K.; Veziroglu, T. N. Curr Sci 2006, 90, 1627.
2. Liu, Z.-P.; Hu, P. J. Am Chem Soc 2002, 124, 5175.
3. Vignais, P. M.; Billoud, B.; Meyer, J. FEMS Microbiol Rev 2001, 25, 455-501.
4. Melis, A.; Zhang, L.; Forestier, M.; Ghirardi, M. L.; Seibert, M. Plant Physiol 2000, 122, 127.
5. Albracht, S. P. J. Biochim Biophys Acta 1994, 1118, 167.

6. Adams, M. W. W. Biochim Biophys Acta 1990, 1020, 115.
7. Adams, M. W. W.; Stiefel, E. I. Science 1998, 282, 1842.
8. Happe, R. P.; Roseboom, W.; Pierik, A. J.; Albracht, S. P.; Bagley, K. A. Nature 1997, 385, 126.
9. Liu, Z.-P.; Hu, P. J. Chem Phys 2002, 117, 8177.
10. Bruschi, M.; Fantucci, P.; De Gioia, L. Inorg Chem 2002, 41, 1421.
11. Bruschi, M.; Fantucci, P.; De Gioia, L. Inorg Chem 2003, 42, 4773.
12. Bruschi, M.; Fantucci, P.; De Gioia, L. Inorg Chem 2004, 43, 3733.
13. Zampella, G.; Bruschi, M.; Fantucci, P.; Razavet, M.; Pickett, C. J.; De Gioia, L. Chem Eur J 2005, 11, 509.
14. Cao, Z.; Hall, M. B. J Am Chem Soc 2001, 123, 3734.
15. Fan, H.-J.; Hall, M. B. J Am Chem Soc 2001, 123, 3828.
16. Greco, C.; Bruschi, M.; De Gioia, L.; Ryde, U. Inorg Chem 2007, 46, 5911.
17. Trohalaki, S.; Pachter, R. Energ Fuel 2007, 21, 2278.
18. Greco, C.; Bruschi, M.; Heimdal, J.; Fantucci, P.; De Gioia, L.; Ryde, U. Inorg Chem 2007, 46, 7256.
19. Greco, C.; Bruschi, M.; Fantucci, P.; De Gioia, L. Eur J Inorg Chem 2007, 13, 1835.
20. Greco, C.; Zampella, G.; Bertini, L.; Bruschi, M.; Fantucci, P.; De Gioia, L. Inorg Chem 2007, 46, 108.
21. Motiu, S.; Dogaru, D.; Gogonea, V. Int J Quantum Chem 2007, 107, 1248.
22. Bruschi, M.; Zampella, G.; Fantucci, P.; De Gioia, L. Coord Chem Rev 2005, 15-16, 1620.
23. Liu, X.; Ibrahim, S. K.; Tard, C.; Pickett, C. J. Coord Chem Rev 2005, 15-16, 1641.
24. Armstrong, F. A. Curr Opin Chem Biol 2004, 8, 133.
25. Rauchfuss, T. B. Inorg Chem 2004, 43, 14.
26. Evans, D. J.; Pickett, C. J. Chem Soc Rev 2003, 35, 268.
27. Chen, Z.; Lemon, B. J.; Huang, S.; Swartz, D. J.; Peters, J. W.; Bagley, K. A. Biochemistry 2002, 41, 2036.
28. Horner, D. S.; Heil, B.; Happe, T.; Embley, T. M. Trends Biochem Sci 2002, 27, 148.
29. Nicolet, Y.; Cavazza, C.; Fontecilla-Camps, J. C. J Inorg Biochem 2002, 91, 1.
30. Lyon, E. J.; Georgakaki, I. P.; Reibenspies, J. H.; Darensbourg, M. Y. Angew Chem Int Ed 1999, 38, 3178.
31. Nicolet, Y.; Piras, C.; Legrand, P.; Hatchikian, E. C.; Fontecilla-Camps, J. C. Structure 1999, 7, 13.
32. Cloirec, A. L.; Best, S. P.; Borg, S.; Davies, S. C.; Evans, D. J.; Hughes, D. L.; Pickett, C. J. Chem Commun 1999, 2285.
33. Rauchfuss, T. B.; Contakes, S. M.; Schmidt, M. J Am Chem Soc 1999, 121, 9736.
34. Lai, C.-H.; Lee, W.-Z.; Miller, M. L.; Reibenspies, J. H.; Darensbourg, D. J.; Darensbourg, M. Y. J Am Chem Soc 1998, 120, 10103.
35. Pierik, A. J.; Hulstein, M.; Hagen, W. R.; Albracht, S. P. Eur J Biochem 1998, 258, 572.
36. Pierik, A. J.; Hagen, W. R.; Redeker, J. S.; Wolbert, R. B. G.; Boersma, M.; Verhagen, M. F.; Grande, H. J.; Veeger, C.; Mustsaers, P. H. A.; Sand, R. H.; Dunham, W. R. Eur J Biochem 1992, 209, 63.
37. Zambrano, I. C.; Kowal, A. T.; Mortenson, L. E.; Adams, M. W. W.; Johnson, M. K. J Biol Chem 1989, 264, 20974.
38. Patil, D. S.; Moura, J. J. G.; He, S. H.; Teixeira, M.; Prickril, B. C.; Der Vartanian, D. V.; Peck, H. D., Jr; Legall, J.; Huynh, B. H. J Biol Chem 1988, 263, 18732.
39. Rusnak, F. M.; Adams, M. W. W.; Mortenson, L. E.; Munck, E. J Biol Chem 1987, 262, 38.
40. Adams, M. W. W. J Biol Chem 1987, 262, 15054.
41. Adams, M. W. W.; Mortenson, L. E. J Biol Chem 1984, 259, 7045.
42. Roseboom, W.; De Lacey, A. L.; Fernandez, V. M.; Hatchikian, E. C.; Albracht, S. P. J. J Biol Inorg Chem 2006, 11, 102.
43. Peters, J. W.; Lanzilotta, W. N.; Lemon, B. J.; Seefeldt, L. C. Science 1998, 282, 1853.
44. Rappe, A. K.; Casewit, C. J.; Colwell, K. S.; Goddard, W. A., III.; Skiff, W. M. J Am Chem Soc 1992, 113, 10024.
45. Dapprich, S.; Komaromi, I.; Byun, K. S.; Morokuma, K.; Frisch, M. J. J Mol Struct (Theochem) 1999, 1, 461.
46. Frisch, M. J.; Trucks, G. W.; Schlegel, H. B.; Scuseria, G. E.; Robb, M. A.; Cheeseman, J. R.; Montgomery, J. J. A.; Vreven, T.; Kudin, K. N.; Burant, J. C.; Millam, J. M.; Iyengar, S. S.; Tomasi, J.; Barone, V.; Mennucci, B.; Cossi, M.; Scalmani, G.; Rega, N.; Petersson, G. A.; Nakatsuji, H.; Hada, M.; Ehara, M.; Toyota, K.; Fukuda, R.; Hasegawa, J.; Ishida, M.; Nakajima, T.; Honda, Y.; Kitao, O.; Nakai, H.; Klene, M. L., X.; Knox, J. E.; Hratchian, H. P.; Cross, J. B.; Bakken, V.; Adamo, C.; Jaramillo, J.; Gomperts, R.; Stratmann, R. E.; Yazyev, O.; Austin, A. J.; Cammi, R.; Pomelli, C.; Ochterski, J. W.; Ayala, P. Y.; Morokuma, K.; Voth, G. A.; Salvador, P.; Dannenberg, J. J.; Zakrzewski, V. G.; Dapprich, S. D., A. D.; Strain, M. C.; Farkas, O.; Malick, D. K.; Rabuck, A. D.; Raghavachari, K.; Foresman, J. B.; Ortiz, J. V.; Cui, Q.; Baboul, A. G.; Clifford, S.; Cioslowski, J.; Stefanov, B. B.; Liu, G.; Liashenko, A.; Piskorz, P.; Komaromi, I.; Martin, R. L.; Fox, D. J.; Keith, T.; Al-Laham, M. A.; Peng, C. Y.; Nanayakkara, A.; Challacombe, M.; Gill, P. M. W.; Johnson, B.; Chen, W.; Wong, M. W.; Gonzalez, C.; Pople, J. A. Gaussian 03, Revision C. 02; Gaussian: Wallingford, CT, 2004.
47. Becke, A. D. J Chem Phys 1993, 98, 5648.
48. Lee, C.; Yang, W.; Parr, R. G. Phys Rev B 1988, 37, 785.
49. Hay, P. J.; Wadt, W. R. J Chem Phys 1985, 82, 270.
50. Wadt, W. R.; Hay, P. J. J Chem Phys 1985, 82, 284.
51. Berendsen, H. J. C.; van der Spoel, D. Comp Phys Commun 1995, 91, 43.
52. Lindahl, E.; Hess, B. J Mol Mod 2001, 7, 306.
53. Popescu, C. V.; Munck, E. J Am Chem Soc 1999, 121, 7877.
54. Rappe, A. K.; Goddard, W. A., III. J Phys Chem 1991, 95, 3358.
55. Peters, J. W. Curr Opin Struct Biol 1999, 9, 670.
56. George, S. J.; Kurkin, S.; Thorneley, R. N. F.; Albracht, S. P. J. Biochemistry 2004, 43, 6808.